

Broad band properties of medium and low L_x/L_b Early Type Galaxies

G. Trinchieri¹, S. Pellegrini², A. Wolter¹, G. Fabbiano³, and F. Fiore⁴

¹ Osservatorio Astronomico di Brera, Via Brera 28, 20121 Milano ITALY

² Dipartimento di Astronomia, Università di Bologna, via Ranzani 1, 40127 Bologna, Italy

³ Harvard-Smithsonian Center for Astrophysics 60 Garden St., Cambridge, MA 02138 USA

⁴ Osservatorio Astronomico di Roma, Via dell'Osservatorio, 00044, Monteporzio Catone, Italy

Abstract. We have measured the spectral properties of five galaxies of low to intermediate L_x/L_b ratios with BeppoSAX and ASCA. A hard component ($kT \sim 4 - 10$ keV) is observed in all galaxies. In NGC 1553 the BeppoSAX data show that this component is extended, and suggest an origin for the emission in the evolved stellar population. In NGC 3115, a point-like source appears embedded in an extended component morphologically similar to the stellar body, suggesting an almost equal contribution from the nuclear region and the binary population. A large central mass concentration and low level optical activity in NGC 3379 argue for a contribution from the nucleus also in this object. However, for both NGC 3115 and NGC 3379, the nuclear emission is at a level well below that observed in other galaxies who host similar nuclear black holes. A second soft ($kT \sim 0.3 - 0.7$ keV) spectral component is needed to fit the data of NGC 1407, NGC 1553 and NGC 4125 over the entire energy range probed ($\sim 0.2 - 10$ keV), best represented by a thermal component with line emission. We discuss possible interpretations of the origin of this component, which however will be better defined only with higher quality data.

Key words: – Galaxies: individual: NGC 1407, NGC 4125, NGC 1553, NGC 3379, NGC 3115 – Galaxies: elliptical and lenticular – Galaxies: ISM

1. Introduction

One of the observational evidences from X-ray data of early type galaxies is the large scatter in the correlation between the X-ray and optical luminosities (Fabbiano, Kim and Trinchieri 1992): at a given optical luminosity, the X-ray to optical flux ratios L_x/L_b may range from those observed in the bulge of M31 and in spiral galaxies, to values $\sim 50 - 100$ times higher. The presence of at least two components, hot gas dominating at high X-ray

luminosities, and the evolved stellar population at faint X-ray luminosities, can explain in part this observational evidence. The spectral characteristics of the emission also reflect the relative importance of these components: already from the limited *Einstein* spectral data, the average emission temperature is larger in galaxies with lower L_x/L_b (Kim et al. 1992), in agreement with the idea of an increasing contribution of hard, individual X-ray sources relative to the hot gas component as the L_x/L_b ratios decrease. An additional very soft component was also found in the lowest L_x/L_b class, possibly due to a $\sim 0.2 - 0.4$ keV interstellar medium or to the collective emission of stellar sources (Pellegrini & Fabbiano 1994).

The ROSAT PSPC and ASCA data confirm the *Einstein* results: a soft ($kT \sim 0.5 - 1$ keV) optically thin emission due to hot gas dominates in X-ray bright objects, and an harder component, with $kT \geq 3 - 4$ keV, most likely associated with the evolved stellar population (Matsuishi et al. 1994; Matsumoto et al. 1997; Buote 1999), or to nuclear activity (Allen, Di Matteo & Fabian 2000; Matsumoto et al. 1997) and present in all galaxies, dominates in X-ray faint objects. In the lowest L_x/L_b class, a very soft component is also measured, with a temperature now well constrained to $\sim 0.2 - 0.3$ keV (Fabbiano et al 1994; Pellegrini 1994; Fabbiano & Schweizer 1995; Kim et al 1996). However, the origin of the very soft component has not been properly understood yet: it could be placed in stellar sources, in X-ray binaries (Irwin & Sarazin 1998), or could be a cooler phase of the ISM: as detailed hydrodynamical simulations show (Pellegrini & Fabbiano 1994), hot gas with the required emission temperature and luminosity can be retained by the galaxies. However, the hot gas temperature is comparable to that of the very soft component only in galaxies with quite shallow potential wells, i.e., with central stellar velocity dispersion $\sigma \leq 200$ km s^{-1} .

More galaxies with intermediate to low L_x/L_b ratios still need to be investigated. We report here the results on the BeppoSAX and ASCA observations of 5 such galaxies. Their general optical properties are summarized in

Send offprint requests to: G. Trinchieri

Correspondence to: ginevra@brera.mi.astro.it

Table 1. General galaxy properties

Name	Type ^a	B_T^0 ^a (mag)	Size ^a (arcmins)	d ^b (Mpc)	$\log L_B$ ^c (L_\odot)	σ ^d (km s ⁻¹)	group ^e (<i>Einstein</i>)	group ^e (<i>ROSAT</i>)
NGC1407	E0	10.71	4.6 × 4.3	34.7	10.99	272	3	3
NGC1553	S0	10.26	4.5 × 2.8	21.5	10.75	200	3	2
NGC3115	S0	9.74	7.2 × 2.5	10.8	10.36	264	1	1
NGC3379	E1	10.18	5.4 × 4.8	13.0	10.35	209	1	–
NGC4125	E6	10.67	5.8 × 3.2	38.0	11.08	232	1-2	2

^a from de Vaucouleurs et al. 1991. B_T^0 is the total B magnitude, corrected for Galactic and internal extinction; the size gives the apparent major and minor axes diameters at the surface brightness level of 25 mag/square arcseconds.

^b distance from Fabbiano et al. (1992), who adopt a Hubble constant of 50 km s⁻¹ Mpc⁻¹.

^c total B-band luminosity L_B , derived using the indicated distance and B_T^0 .

^d central stellar velocity dispersion from McElroy (1995).

^e Group into which the galaxy has been classified on the basis of its $L(0.2-4$ keV)/ L_B ratio (for *Einstein* data, Kim et al. 1992), or its $L(0.5-2.0$ keV)/ L_B ratio (for *ROSAT* data, Irwin & Sarazin 1998). The X-ray faintest galaxies belong to group 1 while the X-ray brightest to group 4. The group boundaries differ in the two papers; in both works they have been chosen so that each group contains roughly the same number of galaxies of the same general spectral characteristics.

Table 1 together with the L_x/L_B group in which they fall according to their soft band X-ray fluxes. The wide energy band and the good spectral resolution of both satellites are suitable to detect and measure separately the amount and spectral parameters of the different emission components. Moreover, the spatial resolution of BeppoSAX at high energies allows us to study the spatial characteristics of the hard component, to determine its extent. We discuss the observations and data analysis in §2-6, we briefly compare the spectral results with those reported in the literature from previous missions and/or different authors in §7, and we discuss the results in §9. In §8 we further discuss a detection at very high energy of a source in the field of NGC 1553, but most likely unrelated to this galaxy.

2. Data Analysis

Five galaxies have been observed with ASCA and BeppoSAX, as summarized in Table 2. While the details of the data analysis are different for each instrument and to a certain degree for each observation, we have followed a similar plan for all. We have first produced smoothed images in the broadest energy band compatible with the statistical significance of the image and with the characteristics of the different instruments (shown in figures 1, 2, 3, 4 and 5 superposed onto the optical images from the Digitized Sky Survey plates¹). We have then determined the extent of the source by comparing the radial profiles of the total emission with the expected background profile, taking into account possible asymmetries in the source morphology, either evident from the present data or with

the help of higher resolution ROSAT images. We have then produced the spectral files, both for the source and its background. We have used the latest release of standard software packages to produce images, spectral photon distributions and ancillary spectral files from the event files, and *IRAF/PROS* and *XSPEC* for the spatial and spectral analysis, respectively. The details of the procedures used for each galaxy are given below.

3. BeppoSAX data

A comprehensive description of the satellite and of the instruments operating on it can be found in Boella et al. (1997a and b); Parmar et al. 1997; Frontera et al. (1997), Manzo et al. (1997) and references therein.

We have used the two imaging instruments on board of BeppoSAX: the Low Energy concentrator spectrometer (LECS), operating in the $\sim 0.1-10$ keV band, with a circular Field of View (FoV) of $\sim 18.5'$ radius; and the Medium Energy concentrator spectrometer (MECS), consisting of 3 identical active units², operating in the $\sim 1.5 - 10$ keV band with a $\sim 28'$ radius FoV. We also report on a detection of emission at higher energies during the observation of NGC 1553 with the Phoswich Detector System (PDS), sensitive in the $\sim 15 - 300$ keV band and co-aligned with LECS and MECS.

As shown in Table 2, NGC 1553 was observed in two separate occasions, about one year apart. The length of each observation is similar, but only two MECS were operating at the time of the second observation, which reflects in the smaller statistics obtained. Each observation is therefore treated independently. The observation of

¹ The Digitized Sky Survey was produced at the Space Telescope Science Institute (STScI) under U.S. Government grant NAG W-2166.

² In May 1997 detector unit 1 of the MECS developed a fault. Since then only units 2 and 3 are operating.

Table 2. Log of the Observations

Object	Instrum	Obs. Dates	On Time
		Beginning - End	(s)
NGC 1407	GIS2	23/08/95 - 24/08/95	34759
	GIS3	23/08/95 - 24/08/95	34755
	SIS0	23/08/95 - 24/08/95	33801
	SIS1	23/08/95 - 23/08/95	33747
NGC 1553	MECS1	16/01/97 - 17/01/97	25880
	MECS2	16/01/97 - 17/01/97	25849
		16/11/97 - 17/11/97	30019
	MECS3	16/01/97 - 17/01/97	25664
		16/11/97 - 17/11/97	29962
	LECS	16/01/97 - 17/01/97	14262
		16/11/97 - 17/11/97	18763
NGC 3115	MECS2	15/05/98 - 16/05/98	35986
	MECS3	15/05/98 - 16/05/98	35952
	MECS2	26/05/98 - 27/05/98	36594
	MECS3	26/05/98 - 27/05/98	36543
	LECS	15/05/98 - 16/05/98	14997
		26/05/98 - 27/05/98	13177
NGC 3379	MECS2	14/12/98 - 17/12/98	99122
	MECS3	14/12/98 - 17/12/98	98749
	LECS	14/12/98 - 17/12/98	34594
NGC 4125	MECS1	26/04/97 - 27/04/97	57128
	MECS2	26/04/97 - 27/04/97	57148
	MECS3	26/04/97 - 27/04/97	56971
	LECS	26/04/97 - 27/04/97	22189
	GIS2	05/04/95 - 05/04/95	38634
	GIS3	05/04/95 - 05/04/95	38634
	SIS0	05/04/95 - 05/04/95	30073
	SIS1	05/04/95 - 05/04/95	21505

NGC 3115 is also split into two segments; however, they are close in time and the same set of instruments is operating, therefore we have merged the two segments in a single set of data. Only the observation of NGC 4125 was completed with all 3 MECS instruments operating.

We have used the event files provided by the SAX Data Center (SDC) that have already been screened with standard criteria, and the blank sky event files as background templates, available from the anonymous ftp SAX-SDC site, that have been also been processed with the same criteria.

Figures 1, 2, 3 and 4 show the smoothed images obtained from MECS and LECS observations for each object superposed onto the optical images. A comparison between the BeppoSAX positions (of the target galaxy and of other sources in the field) and both the optical images and the ROSAT images shows an agreement to within $< 30''$, consistent with the expected BeppoSAX positional error (see Fiore et al. 2000). The possible off-set between LECS and MECS images is also within expectations (see Trinchieri et al. 1999).

The radial profiles of the total emission observed in the MECS instruments, azimuthally averaged in concentric annuli about the X-ray peak, are shown in Fig. 6. In all cases a radial decrease of the emission is observed, followed by a flattening of the profiles at radii in the range $\sim 4' - 8'$, outside of which the profiles are similar to the profiles from the blank sky fields. These have been obtained in the same regions and rescaled for the relative exposure times. In a couple of cases (shown in Fig. 6), the rescaling factors had to be corrected (by $\sim 10\%$) to reproduce the level of the background emission in the field.

Figure 8 shows the comparison of the net emission from the target galaxies detected in the $\sim 2 - 10$ keV band with the MECS Point Spread Function (PSF). The PSF can be described analytically as a function of energy (Boella et al. 1997b), however since it depends on a combination of the effects of the mirror and of the instrument responses, it appears almost independent of energy above a few keV. We have therefore chosen to compare the MECS profiles both with the “worst case” PSF, namely at the softest energy in our band (2 keV), and at an intermediate energy (5 keV).

The LECS data, that extend the energy coverage to lower energies, have a smaller statistical significance due to both the much shorter exposure times (the instrument is operated only during satellite dark time), and the fact that there is only one instrument operating (instead of 2-3). Consequently a detailed spatial analysis is in most cases not feasible. We have therefore disregarded the spatial information from the LECS data, and produced radial profiles only to check the level of the background against the blank sky profiles. For the spectral analysis, we have typically used the same size region determined in the MECS data, centered on the source peak.

3.1. NGC 1553

The source position is $\sim 2/6$ off-axis, since we had tried to include NGC 1549 as well in the field of view. Unfortunately, NGC 1549 is too weak to be detected within this observation with the MECS. A possible enhancement is observed with the LECS at the position of this source, mostly at soft energies, but not with sufficient statistical significance. The off-axis position of NGC 1553 is such that there is no significant degrading of the instrument performances. It has however a significant impact in the handling of the data analysis, mostly in the determination of the background, which is not uniform across the detector³. Therefore, the background for off-axis sources needs to be estimated at the same position in the detector to better account for the additional background produced

³ This is due to the fact that the fluorescence emitted from the two calibration sources located at opposite sides of the detector is probably reabsorbed, and results in enhancement in the internal background near the position of the sources and in the region of the detector that connects the two sources.

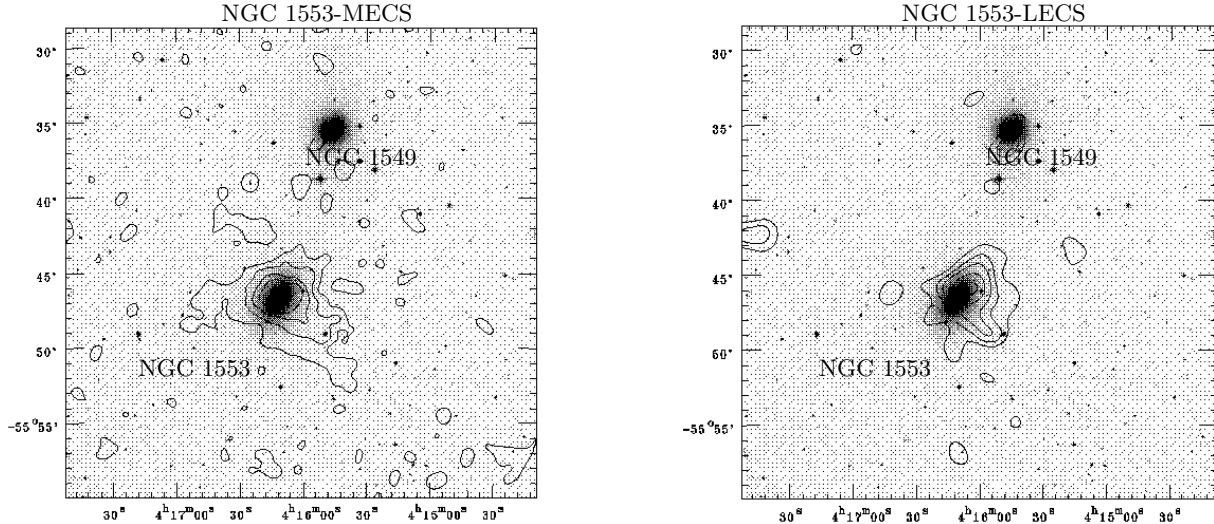


Fig. 1. Contour plots of the SAX images of NGC 1553. LEFT: MECS data, in the 2-10 keV range, smoothed with a Gaussian function with $\sigma=24''$. RIGHT: LECS data, in the 0.1-5 keV range, smoothed with a Gaussian function with $\sigma=32''$.

by these calibration sources (for details, see the “Cook-book” available on line at the SAX-SDC site). Moreover, the source is at different detector positions in the three MECS units. To produce the radial profile of the background shown in Fig. 6, we have summed the azimuthally averaged surface brightness obtained separately for each MECS in concentric annuli, centered as close as possible to the position of the X-ray peak in detector coordinates.

ROSAT data of this galaxy show that the source is extended, and that the emission in a radius of $\sim 5'$ has a general elongation in the NW-SE direction (Trinchieri et al. 1997). A separate source is visible at $\sim 3.6'$ to the SW of the galaxy. The BeppoSAX image also suggests an extended source with a clear elongation in the SW direction, $\sim 4'$ long, visible both in the LECS and in the MECS images. The azimuthally averaged surface brightness (+ signs) decreases out to a radius of $\sim 8'$ and then flattens. However, a significant fraction of the photons outside of $r \sim 2'$ are located in the SW quadrant, presumably due to the source detected with the ROSAT HRI. This is further confirmed by the fact that the comparison between the profiles in the SW quadrants in the first and the second observations suggest that the source has varied in intensity (fainter at the time of the second observation, see Fig. 7).

The comparison between the distribution of the source photons and the BeppoSAX PSF (Fig 8) however confirms the extent of the source, out to a radius $r \sim 6' - 8'$: the source profile is inconsistent with the PSF at all energies

also for azimuthal angles $270^\circ - 180^\circ$ (*i.e.* excluding the SW quadrant).

For the spectral analysis we have therefore considered a source region of $6'$ radius, excluding a circular region of $3'$ at the peak of the SW source (estimated from the ROSAT image as an off-set from the galaxy’s peak). While significantly reducing the contamination, we are left with a peculiarly shaped region, that cannot be properly accounted for to compute the fluxes and similar quantities. However, this should not introduce a bias in the spectral analysis: the files used in the spectral fits that account for photons distributed outside of the source region assume a point source distribution of the photons, which provides an approximation for the true distribution, and we have used a relatively large radius, so that most of the photons are included in the extraction region. The flux however will need to be properly corrected (see § 4).

3.2. NGC 3115

The shape of the X-ray emission follows closely that of the optical galaxy. The MECS isointensity contours appear elongated along the galaxy’s major axis and further indicate possible structure. Only a relatively short ROSAT PSPC observation is available for this object.

The comparison of the radial profile of the total emission, obtained from azimuthally averaged concentric annuli about the X-ray peak, with the blank sky profile

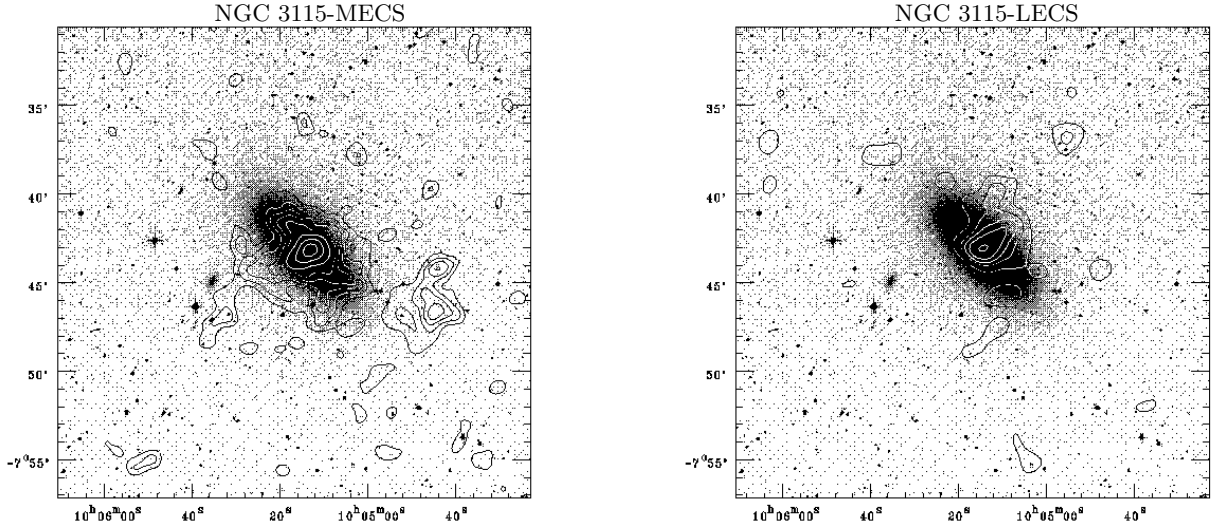


Fig. 2. As in Fig. 1 for NGC 3115.

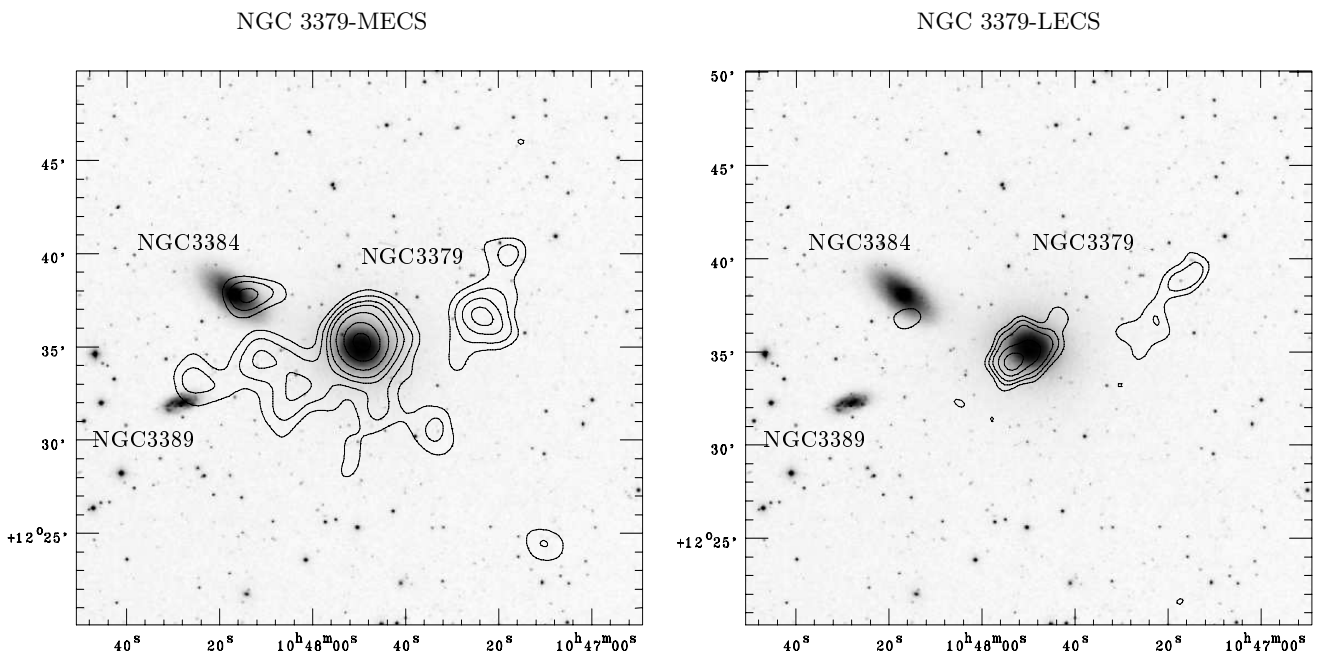


Fig. 3. As in Fig. 1 for NGC 3379.

(Fig. 6) indicates an extension out to $\sim 9'$. However, most of the emission outside $\sim 5'$ is due to the source to the SW, which is most likely unrelated to the galaxy, as shown by the photon distribution obtained excluding a circle of $\sim 2/3$ radius around the SW source (see Fig. 6).

The comparison of the net profile with the PSF is shown in Fig. 8. The NW quadrant (filled dots) is separated from the other three quadrants since it appears less extended than the others and indeed it is consistent with the radial distribution expected from a point source.

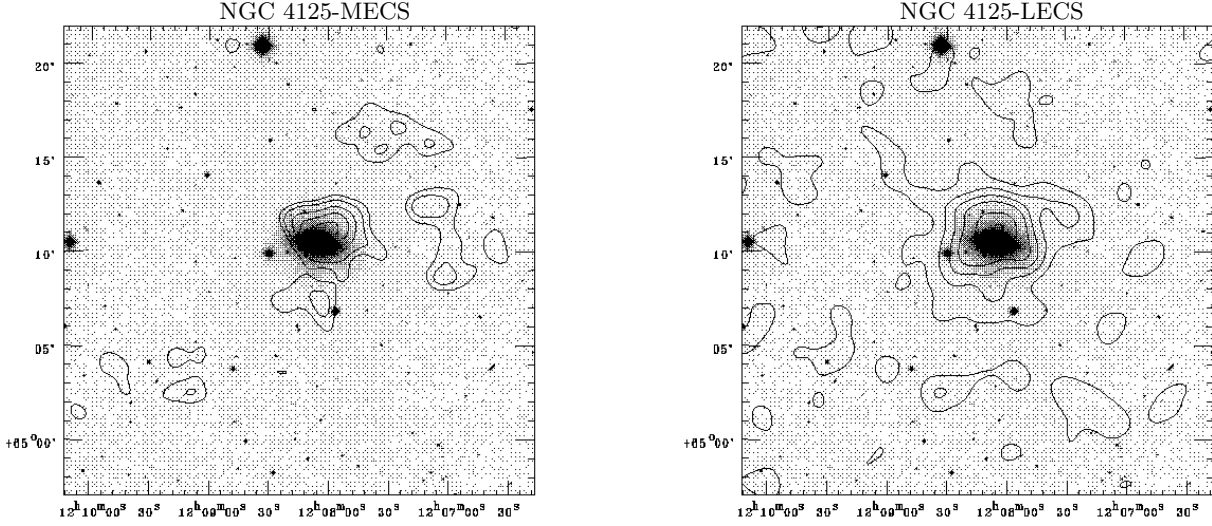


Fig. 4. As in Fig. 1 for NGC 4125.

The other three quadrants are instead significantly more extended and inconsistent with the PSF distribution. This could be the indication of a complex source composed of a point-source embedded in a more extended and somewhat asymmetric emission.

For the spectral analysis however we cannot distinguish the two components and we have therefore used a circle of radius $4'$ as suggested by Fig. 6.

3.3. NGC 3379

The X-ray contours indicate a complex source. Most of the emission is associated with the target galaxy itself, but some emission is present in coincidence with NGC 3384, in the region between NGC 3379 and NGC 3389, and to the West of NGC 3379. This latter source does not coincide with known optical counterparts, but a point-like X-ray source is visible in the ROSAT HRI image of this field. We have therefore excluded this source from the spectral analysis of NGC 3379.

Fig. 6 shows the radial distribution of the total emission from NGC 3379. The azimuthally averaged profile (the interloper to the NW is masked out with a $2'$ radius circle) indicates emission out to a radius $> 8'$. However, the emission outside $\sim 4'$ is due to the extension to the S-SE. In particular, the comparison between the net emission in the Northern and Southern halves with the PSF indicate that the central source is consistent with the photon distribution of a point source. The extension prominent in the SE quadrant is most likely due to the presence

of intergalactic material, but is too faint to be studied with the BeppoSAX data. Although in a different energy band, the ROSAT HRI data also suggest only a nuclear point source (cf. Roberts and Warwick 2000). We have therefore used an extraction radius of $4'$ for the spectral analysis, to maximize the emission from the central source and minimize that from the “diffuse” component.

3.4. NGC 4125

The MECS contour plot in Fig. 4 suggests a possible flattening and an extent towards the south out to a radius of $\sim 5'$, and additional low surface brightness emission is visible outside of the optical image, mostly to the W and NW. LECS data in the same hard band as MECS also suggest the same flattened source, but in the broader band shown in Fig. 4, that includes softer photons, the source appears rounder, most likely due to the larger PSF. The PSPC image (Fabbiano & Schweizer 1995) also shows an equivalent slight distortion of the galactic emission in the EW direction and similar low surface brightness emission at similar distances from the X-ray center.

The azimuthally averaged radial profile of the total emission indicates a sharp decline out to $r \sim 3'$, outside of which the surface brightness flattens and matches reasonably well the shape of the blank sky fields (Fig. 6). The LECS data instead show a slowly decreasing radial profile of the total emission out to a radius of $\sim 6'$, outside of which the profile is consistent with that from the blank sky rescaled for the exposure times only.

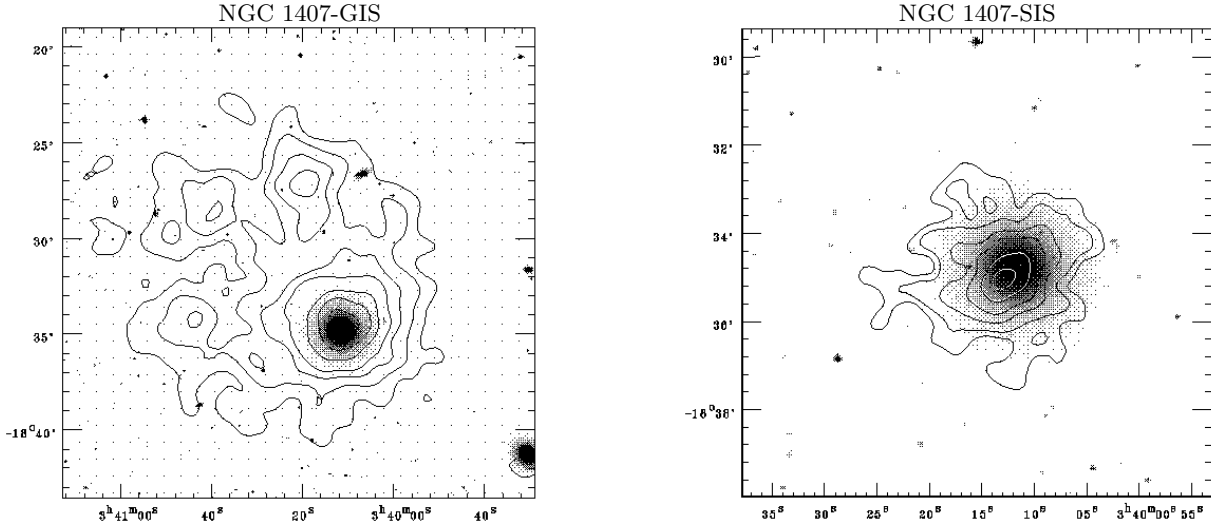


Fig. 5. Contour plots of the GIS (left) and SIS (right) images of NGC 1407. The data have been smoothed with a Gaussian function with $\sigma=13''$.

We have attempted to determine whether the source is extended or compatible with the BeppoSAX PSF, and whether we can measure the distortion apparent in the contour plot. In spite of the poor statistical significance of the observation, the radial profiles shown in Fig. 8 for the full 2-9 keV energy range suggests that there is an excess over the PSF at radii larger than $4'$. This is however due to an excess in the NW quadrant, in the $\sim 4' - 10'$ radii annulus, excess that we detect both at softer (2-3 keV) and harder (3-7 keV) energies.

For the spectral analysis, we have therefore considered a $4'$ radius circle for the extraction region in the MECS, that would exclude the emission in the NW quadrant, and would only consider the emission consistent with the PSF. Since the LECS data indicate source counts out to $6'$ radius, we have used this larger extraction region for this instrument.

4. ASCA data

We have used the “screened” data produced by the REV2 version of the processing. Both sets of focal plane instruments were used (see Table 2). GIS data were obtained in PH mode, and SIS data in BRIGHT mode. Full references to the ASCA instruments and observing modes can be found in the on-line documents at <http://legacy.gsfc.nasa.gov/docs/asca>. Since calibration is poor for energies below 0.5 keV (SIS) and 0.8 keV (GIS), and above 5 keV for SIS, we have restricted

the analysis to energies between 0.5-5 keV and 0.8-10 keV for SIS and GIS respectively.

Each galaxy is discussed briefly below, and the results from the spectral analysis are given in § 5 and tabulated in Table 3.

4.1. NGC 1407

Both Einstein and ROSAT observations of this galaxy show the presence of additional, possibly unrelated, fainter sources around the galaxy, which are also visible in the ASCA images (Fig. 5). Moreover this galaxy is located within a group, so low surface brightness emission from intergalactic gas is expected. The radial photon distribution indicates a slowly decreasing surface brightness emission almost out to the edge of the field (the emission flattens only towards the NE edge off the field, see Fig. 9). We have carefully considered which is the best region to study the emission from this source. In the GIS we have defined a circle of $6'$ radius, that corresponds to a flattening of the surface brightness profile before it further decreases, and is also the recommended size for inclusion of all the flux from a strong point source. With this choice, we can retain a high signal-to-noise and obtain the background locally in an adjacent region that should include the contribution from the group, which we can subtract from the galaxy’s emission. We have also considered a “field” background by choosing a small region in the NE corner of the detector, where the profile shows that the surface brightness is

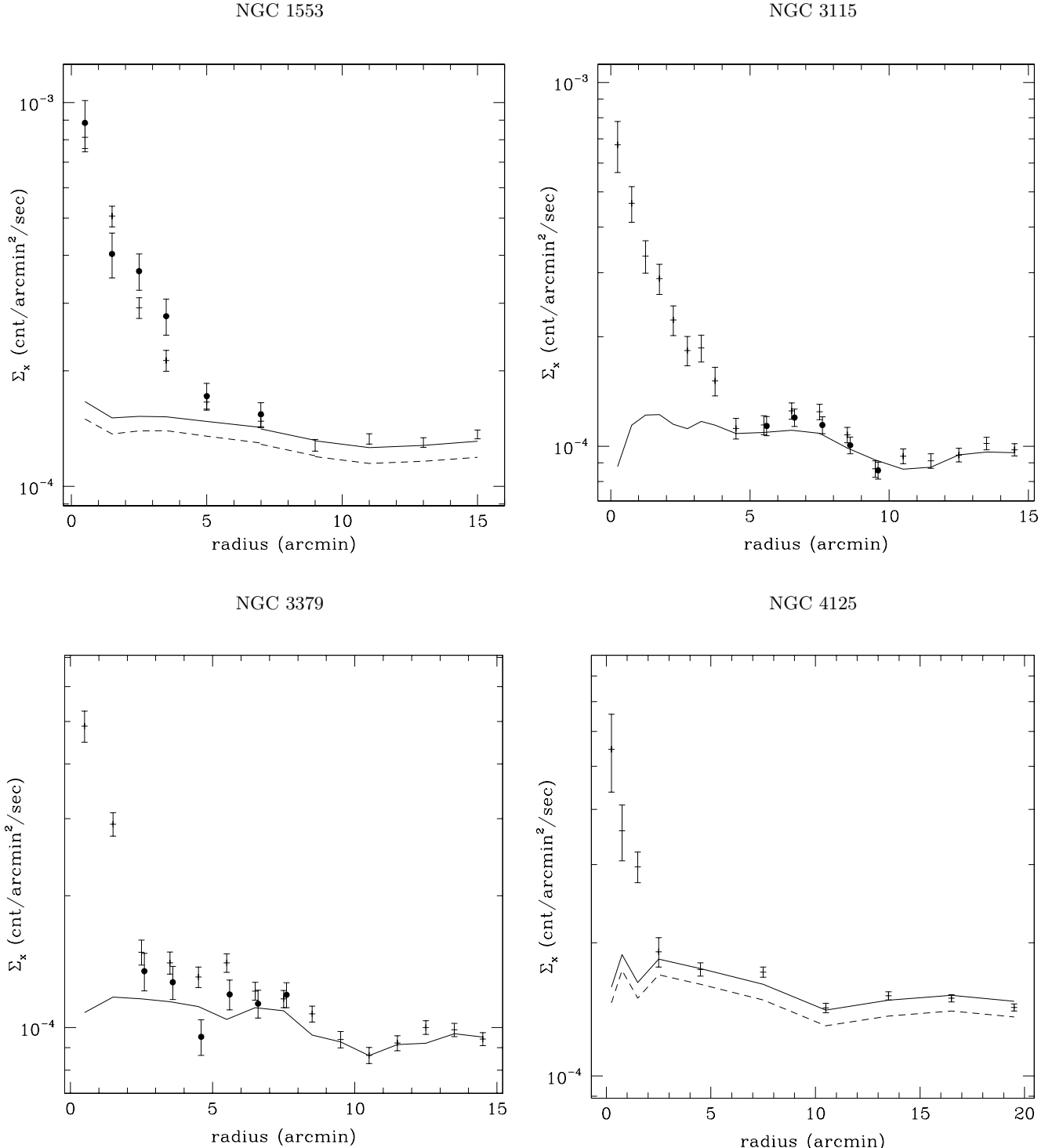


Fig. 6. Radial profile of the total emission (symbols plus error bars) compared to the emission from the blank sky fields (solid line) from the MECS data. The profiles are obtained in concentric adjacent annuli about the X-ray peak and azimuthally averaged, unless otherwise noticed. For NGC 1553 and NGC 4125, two background levels, from the blank sky fields differently normalized to the data, are shown (see text for details). The solid line represents the level assumed. **NGC 1553:** The profiles are obtained in each detector separately and added together. The background profile is centered at the same detector position of the source. Dots: azimuthal angles 270° - 180° . Angles are counterclockwise from North. **NGC 3115:** Filled dots indicate the profile obtained by masking out a circle of ~ 2.3 radius at the position of the SW source (see text). The points are slightly offset in radius for clarity. **NGC 3379:** Filled dots indicate the profile obtained in the Northern half only. A slight offset in radius is added for clarity. In both profiles, the source to the NW is masked out with a circle of radius $r \sim 2'$. **NGC 4125:** two levels for the background profile are shown (see text).

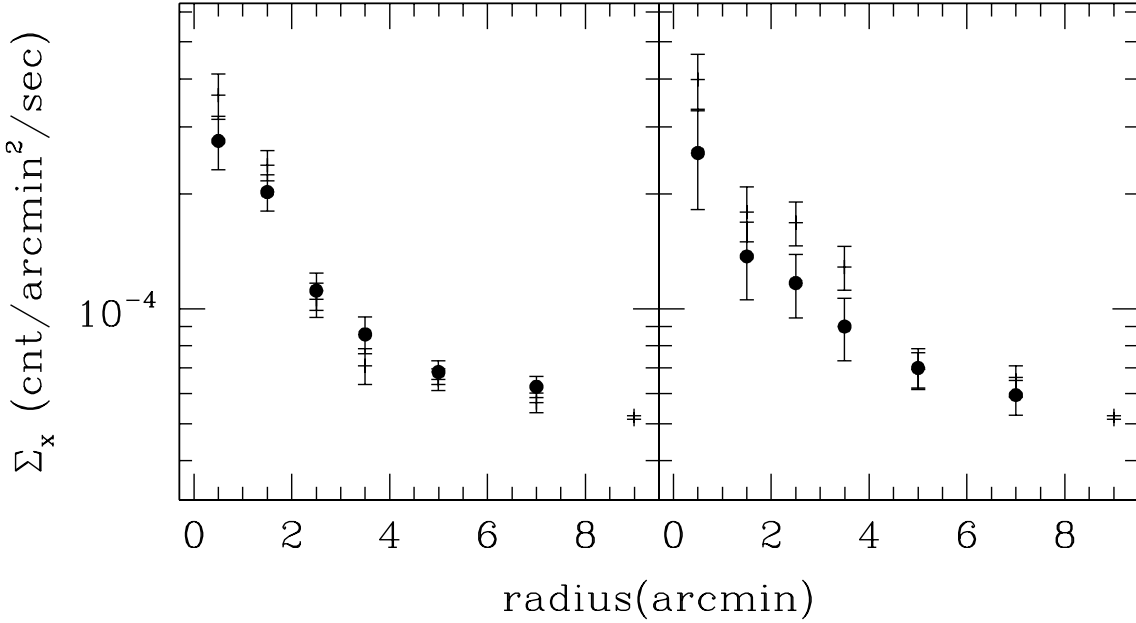


Fig. 7. Comparison of the radial profiles of the total emission in the MECS from different azimuthal sectors in the two observations of NGC 1553. LEFT: angles -90° to 180° are averaged together. Right: angles 180° to 270° are averaged together. + signs are for the first observation, filled circles are for the second observation.

constant with radius. This background was also used to study the emission from the region outside the galaxy (*i.e.* the local background considered above).

For both SIS, we have used a radius of $\sim 3.3'$, the maximum that is allowed by the offaxis position of the source in the detector, that avoids including areas outside of the field of view in the source region. As for the GIS, the background is estimated locally around the source, in a not-concentric annulus as large as it was compatible with the detector size.

While it is true that the ‘unrelated’ sources are included in the background regions, their contribution should not be in excess of $\sim 5\%$, so that they will not significantly affect the background characteristics.

4.2. NGC 4125

As shown by the profile in Fig. 9, source counts are visible out to a radius of $\sim 4'$, then the profile appears to flatten, although a second plateau is visible outside $8'$. The source is relatively centered on the GIS field of view, but not in the SIS. We have therefore used a $4'$ radius circle for the GIS, and chosen the background from a concentric annulus around the source. In the SIS, we have used the maximum radius, of $2.2'$, to avoid regions outside the CCD field of view, and a local background from two regions close to the source.

5. Spectral results

We report in Table 3 the results obtained from the spectral analysis. The spectral data derived in the regions discussed in previous sections have been binned to a coarser energy resolution, to improve on the statistical significance in each bin. We have typically obtained bins in which the net counts are at least 3σ above the background (2σ for the LECS data of NGC 3115 and 2.5σ for the MECS data of NGC 4125). For each observation, we have fitted simultaneously all instruments, fixing the spectral parameters equal for all of them, but we have left the relative normalization as a free parameter, which compensates for different extraction regions in different instruments and cross correlation uncertainties. We have first used a single model with low energy absorption (mostly a thin plasma model [*raymond* in XSPEC], with cosmic abundances fixed at 100%, or a bremsstrahlung). Since in most cases the fit gave a high χ^2_ν or significant residuals in the model-data comparison, we have tried both to relax the constraint on abundances and we have added a second component to the model. Variable abundance fits produced only a partial improvement in χ^2_ν , and gave extremely low, subsolar values. The addition of the second spectral component gave acceptable χ^2_ν values close to 1, even in cases where the statistical significance of the data is poor. A further attempt to lower the χ^2_ν value with a variable abundance model for the soft component does not lead to improvements (see NGC 1407). Since the statistical significance of

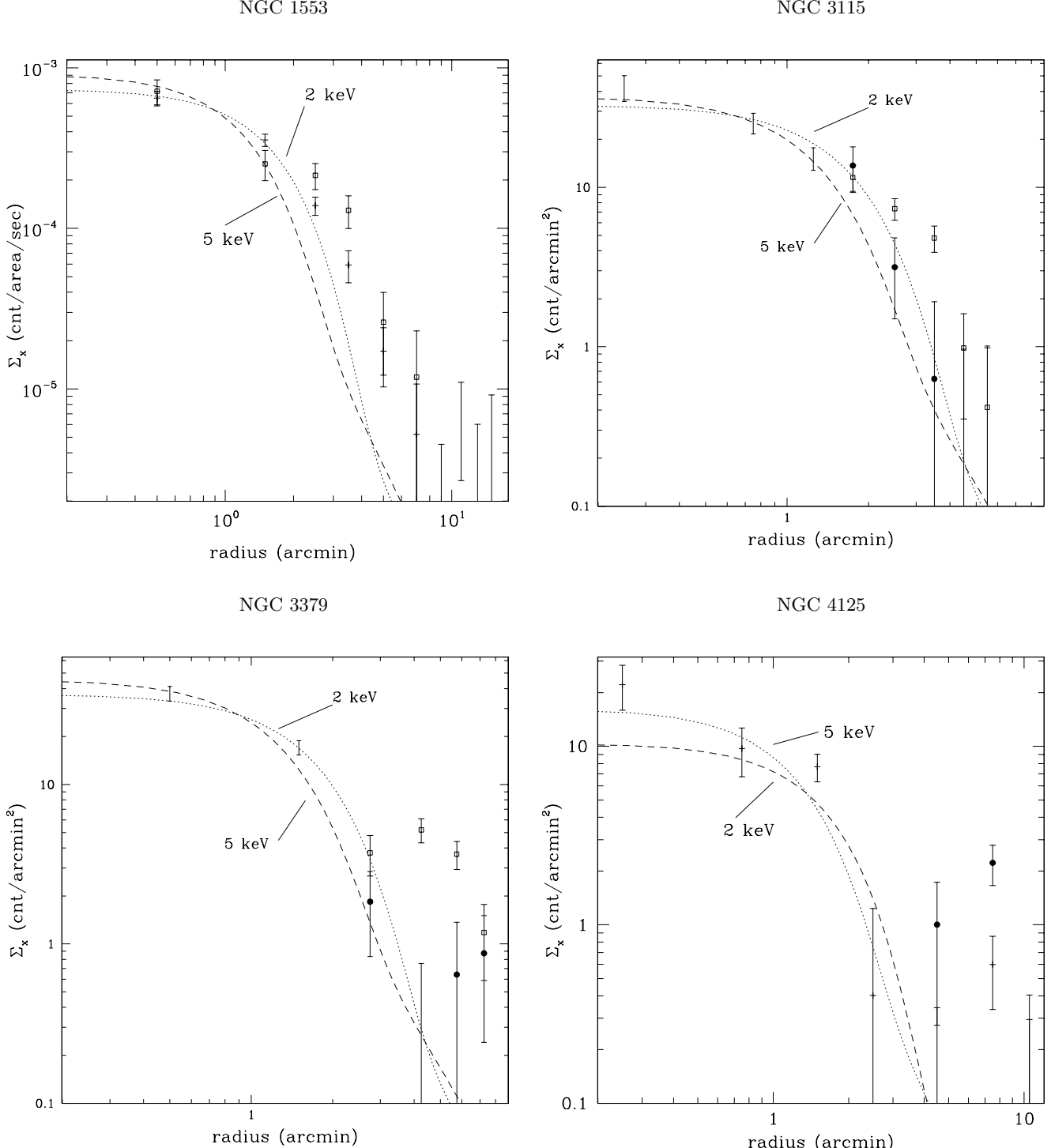


Fig. 8. Radial distribution of the net profiles for the four galaxies (symbols with error bars) detected with the MECS. The profile from the PSF at two energies (dashed and dotted lines) is arbitrarily normalized to the data. **NGC 1553:** the profile is obtained in different angular sectors. + symbols: azimuthal angles 180°-270°; squares: azimuthal angles 270°-180°. Angles are counterclockwise from North. Azimuthal averages outside of 9'. **NGC 3115:** The source to the SW (see text) is masked out with a circle of $\sim 2.3'$ radius. Data within 1.5' are azimuthally averaged. Symbols outside 1.5' indicate: azimuthal angles 0°-270°(boxes); azimuthal angles 270°-360°(filled dots). **NGC 3379:** The profile within a radius of 2' is azimuthally averaged. At larger radii, the profile is obtained in the Southern (open boxes) and Northern (filled dots) halves. The source to the NW is masked out with a circle of radius $r \sim 2'$ (see text). **NGC 4125:** + symbols indicate the azimuthally averaged profile. Filled dots refer to the NW sector only.

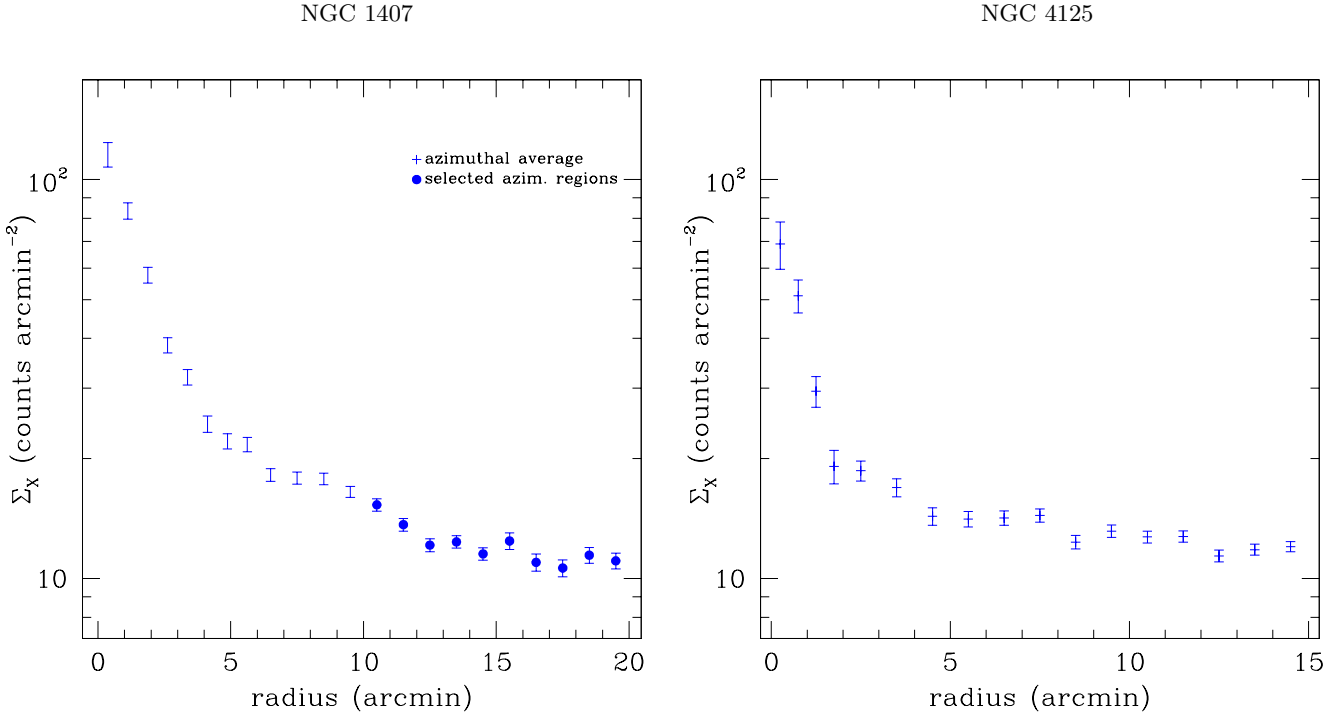


Fig. 9. Radial distribution of the total emission observed with GIS in the 0.8-10 keV energy range. LEFT: data for NGC 1407. In order to avoid regions outside the field of view, only angles -90° to 180° are averaged together at radii $10' < r < 15'$, and angles -30° to 100° outside of $r = 15'$ (angles are counterclockwise from N). RIGHT: data for NGC 4125. The data are azimuthally averaged.

the LECS data is poor, and the SIS data also did not give significant constraints on the low energy absorption value, we have fixed the low energy absorption at the line-of-sight galactic value (Dickey & Lockman 1990).

Individual galaxies are discussed below.

NGC 1407: The results reported in the table refer to the combined SIS and GIS fits to the “galaxy” regions with a local background. We briefly discuss below also the results to the GIS data obtained in the outside region described in § 4.

A single temperature model is not an acceptable fit either to the single data sets or the combined data (see Table 3). When the assumption of fixed abundances is relaxed, the improvement in the χ^2_{min} is significant, but not sufficient to bring it to acceptable values, and the distribution of the residuals confirms that this would be a poor fit. We have then added both a second *raymond* model with 100% cosmic abundances, and a thermal bremsstrahlung: we found that a component at $kT \sim 0.9$ keV, and one at $kT \sim 3-5$ keV give a good fit to the data, for either choice of model for the second component.

The reduced χ^2_{min} indicates that the model is adequate, and therefore there should be no reason to supply more free parameters to the fit. We have nonetheless also tried the same models, but letting the abundance parameter free to vary, to check our results against those of other

authors, who report less than solar best fit abundances (Awaki et al. 1994, Matsumoto et al. 1997). The improvement in χ^2_{min} is actually none, and the abundance parameter cannot be constrained (only $> 10\%$).

We have also substituted the *raymond* with the MEKAL model, for the low temperature component, since this latter should better model the Fe complex at < 1 keV. The results are qualitatively consistent with those reported in Table 3. We find that the best fit values are somewhat different (lower temperatures, as reported by several authors) with equivalent goodness of fit ($\chi^2_\nu \sim 0.94$).

Outside of $6'$ the statistical significance of the data decreases considerably, and the effects of the photons scattered at larger radii because of the Point Spread Function of the ASCA GIS have not been properly modeled (see ASCA on-line documents). However, a fit to the data indicates that the spectrum can be parameterized by a *raymond* spectrum with $kT \sim 1.4$ keV, consistent with intergalactic gas in a group.

NGC 1553: Since the two halves of the observations were obtained with different sets of instruments (see § 3), we had to consider three separate sets of data: MECS data for observation 1 (3 instruments operating), MECS data for observation 2 (2 instruments operating) and LECS data for both observations.

Table 3. Spectral Results

Model	N_H (cm^{-2})	kT_1/Γ (keV)	90% conf. interval	kT_2 (keV)	90% conf. interval	χ^2_ν	D.o.F.
NGC 1407: Combined GIS+SIS							
GIS2: 649 ± 43 counts; GIS3: 852 ± 48 counts; $r=6'$;							
SIS0: 1518 ± 53 counts; SIS1: 1301 ± 47 counts; $r=3.3'$							
1 R	5.5×10^{20}	1.05			2.8	133	
1 R [†]	5.5×10^{20}	0.96			1.7	132	
1 R; 1 B	5.5×10^{20}	0.85	0.83-0.87	3.6	2.7-5.5	1.0	131
NGC 1553—Combined MECS + LECS from both observations							
MECS 305 ± 28 and 207 ± 25 ; LECS 209 ± 21 ; $r=6'$							
1 R	2×10^{20}	3.2			1.9	33	
1 R [‡]	2×10^{20}	3.4			1.9	32	
1 R; 1 B	2×10^{20}	0.26	0.2-0.4	4.8	3-8	1.0	31
NGC 3115—Combined MECS + LECS from both observations							
MECS 391 ± 28 ; LECS 95 ± 15 ; $r=6'$							
1 R	4.5×10^{20}	9.5	5-49		0.8	21	
1 P	4.5×10^{20}	1.58	1.28-1.88		0.8	21	
NGC 3379—Combined MECS + LECS							
MECS 369 ± 31 ; LECS 100 ± 16 ; $r=4'$							
1 R	3.8×10^{20}	6.9	4-24		1.5	15	
1 P	3.8×10^{20}	1.8	1.4-2.1		1.3	15	
NGC 4125 – Combined MECS + LECS							
MECS 103 ± 25 $r=4'$; LECS 136 ± 18 ; $r=6'$							
1 R	2×10^{20}	0.74			2	10	
1 R ; 1 B;	2×10^{20}	0.33	0.25-0.5	3.9	2-12	0.26	8
NGC 4125 – Combined GIS+SIS							
GIS2: 136 ± 19 counts; GIS3: 159 ± 21 counts; $r=4'$;							
SIS0: 385 ± 22 counts; SIS1: 237 ± 17 counts; $r=2.2'$							
1 R	2×10^{20}	0.77			2.7	59	
1 R; 1 B;	2×10^{20}	0.35	*	1.6	*	1.3	47
1 R; 1 B;	2×10^{20}	0.63	*	2.4	*	1.3	47

Note: The models assumed are: *raymond* (R) with abundances fixed at 100% cosmic values unless otherwise indicated; bremsstrahlung (B); power law (P). The 90% confidence interval for temperature(s) or photon index Γ are for 1 interesting parameter (*i.e* they are derived from the $\chi^2_{min}+2.7$ level) and are calculated only for $\chi^2_{min} \sim 1$. The N_H is not well defined by these data. We have fixed it at the line-of-sight galactic value.

[†] The best fit gives abundances of 10% cosmic. [‡] The best fit gives abundances of 0.1% cosmic. * We find two minima of almost equal significance, well outside the 68% error contours. We have not derived errors for these parameters.

The 2-temperature fit improves significantly the values of the minimum χ^2_ν relative to the single temperature model, and indicates temperatures of $kT_1 \sim 0.3$ and $kT_2 \sim 5$ keV. While the need for a two-component model is evident, the requirement of a thin plasma model for the low energy component is not stringent: the χ^2_{min} values are comparable when using a *raymond* (Table 3) or a bremsstrahlung model (best fit temperatures $kT_1 \sim 0.5$ and $kT_2 \sim 11$), although some positive residuals can be seen at energies below 1 keV in the latter case.

NGC 3115 and NGC 3379: A one-temperature component is adequate to fit the data of either galaxies.

Equivalent goodness of fit is obtained from a *raymond*, a bremsstrahlung or a power law model.

NGC 4125: The spectral fit both from the BeppoSAX and from the ASCA data indicates once again that a single temperature model cannot represent the data.

In the 2-temperature fit we find that the soft component must be parameterized by a thin plasma code (*raymond* in this case): assuming a Bremsstrahlung model for the soft component gives a higher minimum $\chi^2_\nu = 2$, and leaves significant positive residuals at energies below 1 keV. Other models we have attempted for the low energy component, like a black-body spectrum, give equally bad distribution of the residuals.

5.1. Fluxes and luminosities of the different components

Table 4 summarizes the best fit fluxes and luminosities of the galaxies discussed here. Total band values as well as the contribution of each component are given in several bands, for easy comparison with previous works. We have converted the MECS or the GIS count rates to fluxes using the best fit spectral parameters reported in Table 3, and the distances in Table 1 to convert these in luminosities.

For NGC 4125, we have used the LECS instead of the MECS data, since the former give a flux consistent with the GIS flux. MECS data give a significantly lower flux. Given the peculiarly shaped extraction region (see § 3), the NGC 1553 flux is derived from the counts listed in Table 3 rescaled to the total expected number, assuming an azimuthally symmetric source (factor of ~ 1.4).

6. Summary of results

The spatial analysis on the MECS data indicates that the distribution of the hard emission in the four galaxies observed with BeppoSAX is different in different cases: NGC 1553 is clearly extended, while NGC 3379 is most likely dominated by a nuclear source. A significant contribution from a point source cannot be excluded by the data of NGC 3115, although a more extended component is also observed. The data of NGC 4125 are not conclusive.

For three sources (NGC 1407, NGC 1553 and NGC 4125) the data require a two component spectrum, with a soft and a hard component, although neither can be determined with high accuracy. The soft component is well parameterized by a thin plasma spectrum, with $kT \sim 0.3 - 0.9$ keV, and in all three cases its contribution is comparable or higher than that of the hard component in the soft energy band.

At hard energies, the extended nature of the emission in NGC 1553 ensures that a nuclear source, if present, does not contribute significantly to the observed luminosity. Both NGC 3115 and NGC 3379 data instead could be parameterized by a power law spectrum, consistent with a significant contribution from a nuclear source.

An intriguing result is provided by the lack of a very soft component in NGC 3115 and NGC 3379, commonly found in the lowest L_x/L_b galaxies (see discussion in § 1). While the poor statistics does not allow us to speculate on whether this is a “significant” result, in the sense of singling out these two galaxies for their lack of a very soft component, the existence of a nuclear component probably further complicates matters. In fact, the soft band ROSAT data of either galaxies do not show a significant contribution from extended components: the galaxies appear rather compact both in the PSPC image of NGC 3115 and in the HRI image of NGC 3379 (cf. Robert & Warwick 2000), suggesting that the nuclear source dominates at all energies. We have estimated the contribution from a soft component allowed by the present data. As discussed before, one component is adequate, and in fact the

addition of a second component to either set of data does not give any additional information: the second component either mimics the parameters of the first component or has a zero normalization. To estimate a possible contribution from a soft component, we have therefore fixed the power law parameters at the best fit values and added a *raymond* with $kT = 0.3$ keV. We find that in either cases a soft component is allowed, and would have an unabsorbed flux $f_x(0.1-2\text{keV}) \sim 1-3 \times 10^{-13} \text{ erg cm}^{-2} \text{ s}^{-1}$ (NGC 3115 and NGC 3379 respectively). We will discuss this further in § 9.

7. Comparison with previous spectral results

The ASCA data of NGC 1407 and NGC 4125 have also been analyzed by Buote & Fabian (1998) and by Matsushita et al. (2000). In the comparison between this and the other two works, we cannot expect equal results, since the spectral analysis is based on different assumptions in all three cases: Buote & Fabian assume a different spectral code for the soft emission (MEKAL) with variable abundances; Matsushita et al. assume a fixed 10 keV temperature for the hard component, and variable abundances for the soft component. However, in spite of the different assumptions, we find good agreement in the best fit soft temperature of NGC 1407, and to within a factor of 2 for the fluxes and luminosities of the different components. For NGC 4125, we cannot properly determine the best fit parameters from the ASCA data, and the Matsushita et al. low temperature component is intermediate between our two best fits.

The ROSAT data of these galaxies have been discussed by Irwin and Sarazin (1998). However, these authors do not perform a spectral analysis of the data, and the hard and soft luminosities they give do not come from two spectral components, but are defined as the luminosity in two narrow bands within the ROSAT band. Therefore they are not directly comparable with the ASCA and BeppoSAX values.

In the PSPC data of NGC 4125, Fabbiano & Schweizer (1995) find two spectral components, at $\sim 0.2 - 0.3$ keV, and $\sim 0.5 - 0.6$ keV and suggest that the harder one is evidence of hot gas. In the BeppoSAX data we do not find the harder component of Fabbiano & Schweizer. However, we notice that the ASCA data do show two minima of equal significance at ~ 0.3 and ~ 0.6 keV (Table 3). A similar result was found in the PSPC data of NGC 1553 by Trinchieri et al (1997), where one of the two components could have an intermediate ~ 1 keV temperature, when the low energy absorption is at the Galactic line-of-sight value.

8. PDS detection

$A \geq 4\sigma$ detection is obtained with the PDS during both observations of the NGC 1553 field. The PDS detec-

Table 4. Fluxes and Luminosities in different bands for the deferent spectral component.

Name		Intrinsic Flux				Intrinsic Luminosity			
		0.1-2 keV	0.2-4 keV	0.5-5 keV	2-10 keV	0.1-2 keV	0.2-4 keV	0.5-5 keV	2-10 keV
NGC1407	T	1.8×10^{-12}	1.9×10^{-12}	1.7×10^{-12}	6×10^{-13}	2.6×10^{41}	2.8×10^{41}	2.5×10^{40}	8.9×10^{40}
	s	1×10^{-12}	9×10^{-13}	8×10^{-13}	5×10^{-14}	1.4×10^{41}	1.3×10^{41}	1.2×10^{41}	7×10^{39}
	h	7.5×10^{-13}	1×10^{-12}	9×10^{-13}	6×10^{-13}	1.1×10^{41}	1.4×10^{41}	1.3×10^{41}	8×10^{40}
NGC1553	T	2.0×10^{-12}	2.0×10^{-12}	1.7×10^{-12}	7×10^{-13}	1.1×10^{41}	1.1×10^{41}	9.7×10^{40}	4×10^{40}
	s	1.3×10^{-12}	1.2×10^{-12}	8×10^{-13}	7×10^{-16}	7×10^{40}	7×10^{40}	5×10^{40}	4×10^{37}
	h	7×10^{-13}	1×10^{-12}	9×10^{-13}	7×10^{-13}	4×10^{40}	5×10^{40}	5×10^{40}	4×10^{40}
NGC3115	P	3×10^{-13}	5×10^{-13}	4×10^{-13}	5×10^{-13}	5×10^{39}	6×10^{39}	6×10^{39}	7×10^{39}
NGC3379	P	3×10^{-13}	4×10^{-13}	3×10^{-13}	3×10^{-13}	6×10^{39}	7×10^{39}	7×10^{39}	6×10^{39}
NGC4125	T	7×10^{-13}	7×10^{-13}	6×10^{-13}	1×10^{-13}	1.2×10^{41}	1.2×10^{41}	1×10^{41}	2.4×10^{40}
	s	5×10^{-13}	5×10^{-13}	4×10^{-13}	1×10^{-15}	9×10^{40}	8×10^{40}	7×10^{40}	2×10^{38}
	h	2×10^{-13}	2×10^{-13}	2×10^{-13}	1×10^{-13}	3×10^{40}	4×10^{40}	4×10^{40}	2×10^{40}

Total (T), soft (s), hard (h) components from the two-component fits from Tables 3 are given. Power law fits are used to compute the flux of NGC 3115 and NGC 3379. All quantities have been corrected for the Galactic line of sight value of N_H . Values are from MECS data (GIS for NGC 1407) except for NGC4125, where the LECS values are used, since they are comparable to the GIS values. NGC 1553 values have been rescaled by a factor of 1.44 to compensate for the area that has been masked out (see text).

tor is a non-imaging instrument with an hexagonal FoV with $\text{FWHM} \sim 75'$ (Frontera et al. 1997 and references therein). Given the very large field of view of this instrument and the lack of spatial resolution, the identification of the PDS source is not straightforward.

We have used the PHA files provided by the SDC to study the origin of this emission, and in particular to understand whether the source detected with the PDS could be related to the galaxy.

We have first tried to fit the PDS data together with MECS and LECS. The best fit model found for the LECS+MECS combination could fit the PDS data, but would require a normalization factor of ~ 70 for the PDS data, well outside the expected value of ~ 1 ($\sim 0.8 - 0.9$ for MECS-PDS and $\sim 0.8 - 1.2$ for LECS-PDS). This indicates a very large excess over the emission expected from the galaxy at higher energies, and argues against an association with it.

We have therefore searched for other plausible candidates in the PDS FoV. As shown by the MECS data, there are virtually no other sources in the field, also when we consider hard energies only (above 4 and 6 keV to account for heavily absorbed sources), and a similar search in the 2 degree PSPC field centered on NGC 1553 also suggests that all of the ROSAT sources in the area would have been in the MECS FoV, indicating that they are either very soft or too faint to be detected by BeppoSAX. It is therefore highly unlikely that any of these is the counterpart of the PDS source. On the other hand, it is also unlikely that the combination of all these sources causes the PDS detection: NGC 1553 is by far the brightest at high energies, and the discrepancy in flux is too large to be accounted by the sum of a few much fainter sources.

We have searched for neighbouring sources in an area of 1.5 degree radius around NGC 1553 in X-ray catalogs. We have found entries only in the catalogs from ROSAT and *Einstein* data. In the RASS source list we found 8 sources, two of which are contained in the MECS FoV (one in fact is NGC 1553 itself). The brightest one, at $\sim 1^\circ$ NE, coincides with NGC 1566, which is also detected in the *Einstein* Slew Survey. This is the only possible source of emission since it is a Seyfert galaxy, with a variable soft X-ray flux measured by *Einstein* up to $f_{0.2-4.0} \sim 2.2 \times 10^{-11}$ $\text{erg cm}^{-2} \text{s}^{-1}$ (Fabbiano, Kim and Trinchieri 1992).

BeppoSAX observations of NGC 1566 do not exist, and we cannot therefore unambiguously establish that the PDS detection is indeed due to the emission of NGC 1566. One of the main problems is that all observations available from previous X-ray missions (*Einstein* and ROSAT) are in a much softer band than the PDS, so that comparison of the flux in a common band has to rely on the spectral parameters assumed, that have to be extrapolated over more than a decade in energy. Since the spectral capabilities of both previous missions and the PDS instrument, with the low statistical significance of the data, are poor, this comparison is very uncertain. We have applied different spectral models to the PDS data and derived band fluxes for comparison with previous results: a) the best fit power law $\Gamma=2.3$ determined from the ROSAT data (Ehle et al. 1996) gives $f_{2-10} \sim 3 \times 10^{-11} \text{ erg cm}^{-2} \text{s}^{-1}$ and $f_{0.2-4.0} \sim 1 \times 10^{-10} \text{ erg cm}^{-2} \text{s}^{-1}$ b) the canonical power law slope for Sey 1, $\Gamma=1.7$, gives $f_{2-10} \sim 2 \times 10^{-11} \text{ erg cm}^{-2} \text{s}^{-1}$ and $f_{0.2-4.0} \sim 2 \times 10^{-11} \text{ erg cm}^{-2} \text{s}^{-1}$.

Given all of the uncertainties in the spectral parameters, the extrapolation from the PDS to the softer energy band is consistent with the identification of the PDS

source with NGC 1566, in particular if the source was in a high flux state, since the above estimates do not take into account the degradation of the PDS response at the large off-axis position of the galaxy.

9. What is the origin of the X-ray emission in early-type galaxies?

The presence of at least 2 components in the X-ray spectra of early type galaxies is now well established for all galaxies spanning the whole range of L_x/L_b ratio, although the origin of these component might be different, as will be discussed later.

Even though the quality of the present data does not allow us to derive very precise spectral parameters for the galaxies studied here, we can discuss their properties in light of these results together with current discussions in the literature.

When the full spectroscopic range of $\sim 0.2 - 10$ keV is taken into account, the need of at least two components to the model fit becomes quite stringent. As already noticed often in the literature (cf. Buote 1999 and references therein), the present data stress the importance of including the contribution of the harder spectral component at soft energies, even though it might not be possible to measure its strength or detailed characteristics, to avoid a faulty interpretation of the data.

A thin plasma spectrum is most likely the best model to fit the low temperature component in these intermediate and low L_x/L_b objects. For NGC 1407 and NGC 4125 a simple thermal bremsstrahlung fails to reproduce the data at energies below 1 keV, indicating either the need of an additional component or of line emission. Lines are also required to model the low energy component of X-ray bright objects, interpreted as due to the emission of hot gas, although the detailed characteristics (mostly abundances), of the lines have not been unambiguously determined at the present time. In the lower L_x/L_b galaxies, the presence of lines cannot be used to firmly identify the soft component with emission from hot interstellar gas, since line emission below ~ 1 keV has also been found in the spectra of Galactic low mass binaries (Her X-1 and 4U1626-67, Oosterbroek et al. 1997; Owens et al. 1997).

In fact the presence of hot gas at the low end of the X-ray luminosity distribution has been recently challenged by Irwin and Sarazin (1998) who, based on the similarity between the X-ray colors (in the ROSAT band) of low X-ray luminosity galaxies and the bulge of M31, NGC 1291 and galactic low Mass X-ray Binaries (LMXB), have suggested that the LMXB sources could account for the whole spectrum of low L_x/L_b galaxies. BeppoSAX and ASCA data on the bulge of M31 (Trinchieri et al. 1999), together with a new analysis of ROSAT PSPC data (Irwin & Bregman 1999), have confirmed the need of a soft component to model the 0.1-10 keV spectrum. The spatial evidence from high resolution X-ray images indicates that a major

fraction of the emission is resolved into individual sources, while a smaller percentage could be accounted for by either a population of lower luminosity sources or by a truly diffuse component (the fraction attributed to each component however is different in the *Einstein* and ROSAT data, see Trinchieri and Fabbiano 1991 and Primini et al. 1993). This argues against a significant contribution from an ISM in the bulge of M31, and suggests that the soft emission detected could indeed be attributed to the low mass binary population. However, whether LMXBs could account for *all* of this component, and whether the same applies to low luminosity early type galaxies as well is still a very open question: 1) the relative contributions of the soft and hard components in M31 do not appear to be the same as those measured in early type galaxies, at least based on the evidence given by BeppoSAX and ASCA (Trinchieri et al. 1999; however, see Irwin and Bregman 1999); 2) Kim et al. (1998) discuss the positive detection of gas in NGC 1316, one of the low L_x/L_b early type galaxies, which further reinforces the need of more than just binaries in these objects; 3) Borozdin & Priedhorsky (2000) argue that the spectra of the diffuse emission and of the binary sources in M31 differ, suggesting that the soft component is to be attributed all to the unresolved component and not to the LMXB population.

Figure 10 shows the comparison between the soft emission observed in the bulge of M31 with BeppoSAX, ASCA and ROSAT and that observed in the lowest L_x/L_b early type galaxies. In all objects where the soft component has been measured there is excess emission over even the higher estimate of the expected contribution from binary sources, suggesting that an additional component should be present or that the binaries contribute a higher proportion in the lowest L_x/L_b galaxies. Better quality data however, such as will be provided by *Chandra* and XMM-Newton observations, are needed to understand the nature of the soft emission in early type galaxies.

At the opposite end of the spectrum, the origin of the emission that dominates at higher energies remains unclear. The evolved stellar population in early type galaxies should give rise to hard emission proportional to the stellar content, similar to what is observed for late type galaxies. In addition, there could be emission from a nuclear source, although in most cases a further requirement that the source is heavily obscured is necessary when the high resolution data at soft energies do not show evidence of an unresolved nuclear source. If the evolved stellar population is responsible, we expect the spectral characteristics of the hard component to be similar to those of the LMXB in our Galaxy, in M31 and to the integrated emission in late type galaxies, where this component is thought to dominate. We also expect its luminosity to be almost linearly correlated to the optical luminosity, as in the spiral galaxy sample (Fabbiano et al. 1992), indicating that a constant fraction of stars has evolved in the compact binary systems. Moreover, the emission should be clearly

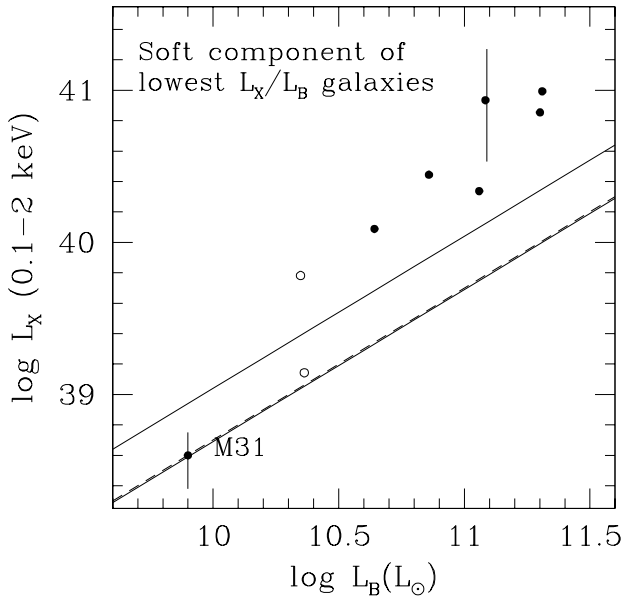


Fig. 10. Correlation between the optical (B-band) and soft X-ray luminosity (0.1-2 keV band) in the lowest L_x/L_b early type galaxies (i.e., those belonging to group 1, as defined in Table 1). The solid lines represent the expected contribution from LMXBs estimated by Irwin & Bregman (1999) from an *ASCA+ROSAT* analysis of the bulge of M31; the lines shown include the extreme contributions allowed by different spectral models that are considered equally good by the authors. The dashed line is normalized to the estimate of the emission of a very soft component in the bulge of M31 from *BeppoSAX* data (Trinchieri et al. 1999). Data are from this paper for NGC4125, Fabbiano et al. (1994) for NGC 4382 and NGC 4365, Kim et al. (1996) for NGC 1316, Pellegrini (1994) for NGC 5866, and Matsushita et al. (2000) for NGC 4697. The open symbols indicate the estimates of the soft component in NGC 3115 and NGC 3379 (see text). Errors on the flux are given for NGC 4125 and M31 and are estimated from the 90% uncertainties on the normalization of the soft spectral component.

extended, and follow the radial distribution of the optical light. Signatures of nuclear activity at other wavelengths combined with no spatial extension and appropriate spectral characteristics would instead point to a nuclear source in the galaxy.

The existence of the hard component was first suggested on the basis of very crude spectral data from the *Einstein* IPC (Kim et al. 1992) but was measured for the first time with *ASCA* data in an increasingly large number of galaxies (Matsushita et al. 1994; Matsumoto et al. 1997). However, there is to date no firm determination of its spectral characteristics: in most cases (and the *BeppoSAX* and *ASCA* data presented here are consistent with this), either a power law or a thermal model can be

used to parameterize its spectrum equally well (see also Allen et al. 2000, Table 3).

The temperature measured for the high energy component (kT in the range $\sim 3 - 10$ keV, see Table 3) is consistent with the spectral characteristics of the LMXBs in our Galaxy (van Paradijs 1998) and of the bulge and several sources of M31 measured with *BeppoSAX* (Trinchieri et al. 1999). For power law spectra, the indexes reported in Table 3 appear to be consistent with the canonical slope of Seyfert galaxies (see also Matsumoto et al. 1997, Buote & Fabian, 1998). This is not consistent with the results for a sample of high X-ray luminosity galaxies studied by Allen et al. (2000), whose hard component appears to have a flatter spectrum. However, the flat component in the very high luminosity objects is in general a small fraction of the emission in the hard band and appears to dominate only at very high energies (above 5 keV in the spectrum of M87, see Fig. 2 in Allen et al. 2000),

The spatial analysis of the *BeppoSAX* data indicates that the high energy emission of NGC 1553 is extended and that a point source and an extended component account for the emission in NGC 3115 (Fig 8). This argues against a dominant contribution from the nucleus in these two objects (although in NGC 3115 the two could contribute equally). The *BeppoSAX* data on a third object, NGC 3923 (Pellegrini 1999), also argue against nuclear emission. For the other two galaxies observed with *BeppoSAX*, NGC 3379 and NGC 4125, the spatial evidence is not as conclusive: there is an indication of excess emission over the PSF, but mostly due to other, possibly unrelated, components. However, a nuclear contribution is likely to be important in NGC 3379, since Roberts and Warwick (2000) report the detection of a single nuclear source in this galaxy from HRI data.

We therefore can exclude a nuclear origin of the hard emission only for NGC 1553 (and NGC 3923), for which a stellar origin of the emission is most likely. From the spatial analysis of NGC 3115 we expect a mixture of nuclear plus stellar component in this galaxy. A large contribution is expected from the nucleus of NGC 3379.

We have tried to compare the characteristics of the hard emission of these galaxies to those previously reported in the literature, in an attempt to discriminate between binary and nuclear emission. In Fig. 11 we present a plot similar to Fig. 7 of Buote & Fabian (1998), but we have included *only* galaxies for which the hard component has a temperature higher than ~ 3 keV, so that we are sure we are not including the contribution from the hot gas, or an hotter phase of the ISM (see Buote & Fabian 1998).

As shown by the figure, the scatter in the points is relatively large and the present galaxies are in very good agreement with the other early type galaxies from the literature. All are consistent with what might be expected from emission from the binary population (sketched by the lines in the figure, derived by Canizares et al. (1987), based

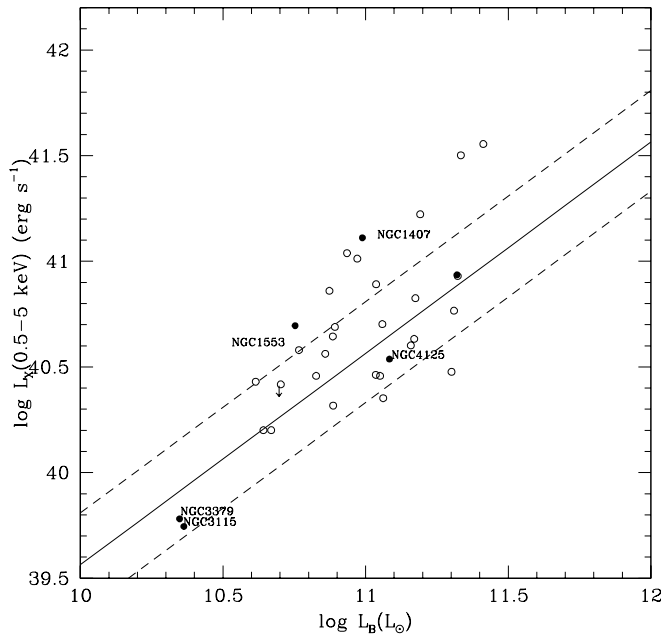


Fig. 11. Correlation between the optical (B-band) luminosity and that of the hard component, with temperature ≥ 3 keV, for early type galaxies. The galaxies studied here are labeled with their names. Data for the other galaxies are from Buote and Fabian (1998), Kim et al. (1996), Matsumoto et al. (1997), Matsushita et al. (2000). The nameless dot is NGC3923, also studied with BeppoSAX and also found extended in the hard band (Pellegrini 1999). The solid line represents the expected contribution from the binary component (Canizares et al. 1987); this estimate is coincident with that obtained from ASCA data by Matsumoto et al. (1997). The dashed lines enclose the expected scatter/uncertainty for the binary contribution (Canizares et al. 1987).

on globular clusters and sources in the bulge of M31), as already noticed by Buote & Fabian (1998). The extended nature of the emission in NGC 1553 and NGC 3923 guarantees that these estimates are indeed reasonable, as shown by their positions in the plot. NGC 1407 appears to be outside the range of the binary sources. However, since it hosts a compact, flat-nuclear source (Disney & Wall 1977, Dressler & Wilson 1985) and it is located at the center of a small group, we cannot exclude additional emission from either of these components. A similar reasoning can be applied to other galaxies in the same part of the diagram.

Stellar kinematics for two of the present galaxies, NGC 3115 and NGC 3379, testify to the presence of a central mass concentration of $M \sim 10^8 - 10^9 M_\odot$ (Kormendy et al. 1996; Emsellem 1999, Gebhardt et al. 1996; 2000; Magorrian et al. 1998). NGC 3379 has been classified as a LINER 2 in the spectroscopic survey to search for nuclear activity

conducted by Ho et al. (1997). A contribution from the nuclei could therefore be expected in these two objects. However, their hard components are within the range expected for the binaries contribution (Fig. 11), and their luminosities are well below what has been observed in other galaxies who host a similar or even lower mass nuclear black holes, *e.g.* NGC 4258 (Fiore et al. 2000), with an X-ray luminosity $L_x(2 - 10) \sim 10^{41}$ erg s $^{-1}$ and a black hole mass of $\sim 4 \times 10^7 M_\odot$, or the Sombrero galaxy, with $L_x(0.1 - 2.4) \sim 3.4 \times 10^{40}$ erg s $^{-1}$ (Fabbiano & Juda 1997).

If we assume a substantial contribution from the nucleus, then the contributions from binaries alone is lower (from the spatial analysis, a factor of about 2 for NGC 3115, most likely more for NGC 3379), and could fall below the estimates shown in Fig. 11 for the binary contribution. However, given the relatively large range spanned by the points, the poor knowledge of the properties of this component in early type galaxies and the lack of points at the same low optical magnitude of these galaxies, we cannot realistically speculate on whether this would make the high energy emission from these two galaxies peculiar relative to the other objects.

We further notice that the (unknown) intrinsic scatter in the plot could be enhanced both by the limited quality of the data available and by the limited information available on the detailed properties of these sources. Different assumptions on the spectral models, the uncertainties even within a single set of spectral model and the presence of several components (nuclei, binaries, group emission), which cannot be discarded both in different objects and within the same object with the present data, could introduce factors of a few in the estimates of the source luminosities (as already remarked in §7).

We can therefore only conclude that on average we expect that a large fraction of the hard emission in early type galaxies originates from the evolved stellar population, as seen in later types. Once again, the spatial and spectral capabilities of *Chandra* and XMM-Newton are required to properly measure the characteristics of this component and therefore better understand its origin.

Acknowledgements. This work was partially supported by the Italian Space Agency. GT thanks Prof. Trümper and the MPE staff for their hospitality and support while part of this work was done. This research has made use of the NASA/IPAC Extragalactic Database (NED) which is operated by the Jet Propulsion Laboratory, California Institute of Technology, under contract with the National Aeronautics and Space Administration.

References

- Allen, S.W., Di Matteo, T. & Fabian, A.C. 2000, MNRAS 311 493
- Awaki, H., Mushotzky, R., Tsuru, T., Fabian, A. C., Fukazawa, Y., Loewenstein, M., Makishima, K., Matsumoto, H., Matsushita, K., Mihara, T., Ohashi, T., Ricker, G. R., Serlemitsos, P. J., Tsusaka, Y., Yamazaki, T. 1994, PASJ 46L, 65.

Boella, G., Butler, R. C., Perola, G. C., Piro, L., Scarsi, L., Bleeker, J. A. M. 1997a, AAS 122 299

Boella, G., Chiappetti, L., Conti, G., Cusumano, G., Del Sordo, S., La Rosa, G., Maccarone, M. C., Mineo, T., Molendi, S., Re, S., Sacco, B., Tripiciano, M. 1997b AAS 122 327

Borozdin, K.N. & Priedhorsky, W.C. 2000 astroph

Buote, D.A. 1999 MNRAS 309, 685

Buote, D.A. & Fabian A.C. 1998 MNRAS 296 977

Canizares, C.R., Fabbiano, G., Trinchieri, G. 1987 ApJ 312, 503

Dickey, J.M., Lockman, F.J. 1990, ARAA 28, 215

Disney, M. J., Wall, J. V 1977 MNRAS 179, 235

Dressel, L. L., Wilson, A. S 1985 ApJ 291 668

Ehle, M. Beck, R., Haynes, R.F., Vogler, A., Pietsch, W., Elmouttie, M., Ryder, S. 1996, AA 306, 73.

Emsellem E. 1999 astro-ph/9910006

Fabbiano, G. Kim, D-W. and Trinchieri, G. 1994 ApJ 429, 94

Fabbiano, G., Kim, D-W., and Trinchieri, G. 1992, ApJS 80, 645

Fabbiano, G., Juda, 1997 ApJ 476, 666

Fabbiano, G., Schweizer F. 1995 ApJ 447 572

Fiore, F., Giommi, P., Vignali, C., et al. 2000 MNRAS submitted

Frontera, F., Costa, E., Dal Fiume, D., Feroci, M., Nicastro, L., Orlandini, M., Palazzi, E., Zavattini, G. 1997 AAs 122 357

Gebhardt, K., Richstone, D., Ajhar, E. A., Lauer, T. R., Byun, Y.-I., Kormendy, J., Dressler, A., Faber, S. M., Grillmair, C., Tremaine, S. 1996, ApJL, 471, L79

Gebhardt, K., Richstone, D., Kormendy, J., Lauer, T. R., Ajhar, E. A., Bender, R., Dressler, A., Faber, S. M., Grillmair, C., Magorrian, J., Tremaine, S. 2000 AJ 119, 1157

Ho L.C., Filippenko A. V., Sargent W. L. W., Peng C. Y. 1997, ApJS 112, 391

Irwin J.A and Bregman J.N 1999 ApJL 510 L21

Irwin J.A. and Sarazin C. L. 1998 ApJ 499 650.

Kim D-W., Fabbiano G., & Trinchieri G. 1992 ApJ 393, 134.

Kim D.-W. & Fabbiano, G. 1995 ApJ 441, 182.

Kim D.-W., Fabbiano G., Matsumoto H., Koyama K., Trinchieri G. 1996 ApJ 468, 175

Kim D.-W., Fabbiano G., Mackie G. 1998, ApJ. 497, 699.

Kormendy, J., Bender, R., Richstone, D., Ajhar, E. A., Dressler, A., Faber, S. M., Gebhardt, K., Grillmair, C., Lauer, T. R., Tremaine, S. 1996 459, L57

Manzo, G., Giarrusso, S., Santangelo, A., Ciralli, F., Fazio, G., Piraino, S., Segreto, A. 1997 AAS 122 341

Matsumoto, H., Koyama, K., Awaki, H., Tsuru, T., Loewenstein, M., Matsushita, K. 1997 ApJ 482 133

Matsushita, K., Makishima, K., Awaki, H., Canizares, C. R., Fabian, A. C., Fukazawa, Y., Loewenstein, M., Matsumoto, H., Mihara, T., Mushotzky, R. F., Ohashi, T., Ricker, G. R., Serlemitsos, P. J., Tsuru, T., Tsusaka, Y., Yamazaki, T 1994 ApJ 436L 41

Matsushita, K. et al . (2000) astroph

Magorrian, J., Tremaine, S., Richstone, D. et al. 1998 AJ 115, 2285

McElroy D.B. 1995, ApJs 100, 105

Oosterbroek T., Parmar A.N., Martin D.D.E., Lammers U. 1997 AA 327 215

Owens A., Oosterbroek T., Parmar A.N. 1997 AA 324 L9

Parmar, A. N., Martin, D. D. E., Baudaz, M., Favata, F., Kulkers, E., Vacanti, G., Lammers, U., Peacock, A., Taylor, B. G 1997 AAS 122 309

Pellegrini, S. 1994, A&A 292, 395

Pellegrini, S. & Fabbiano, G. 1994, ApJ 429, 105

Pellegrini, S. 1999, A&A 343, 23

Primini F. et al 1993, ApJ 410 615

Roberts, T.P.& Warwick, R.S. 2000, MNRAS 315, 98

Trinchieri, G., Fabbiano, G. 1991, ApJ 382, 82 310, 637

Trinchieri, G., Kim, D-W., Fabbiano, G., & Canizares, C.R.C. 1994, ApJ 428, 555

Trinchieri, G., Noris, L., diSerego Alighieri, S. 1997 AA 326, 565

Trinchieri, G., Israel, G.L., Chiappetti, L., Belloni, T., Stella, L., Primini, F., Fabbiano, P., Pietsch, W. 1999, AA 353, 487

van Paradijs J. 1998, "The many faces of neutron stars", R. Buccieri, J. van Paradijs, M.A. Alpar (eds), Kluwer Academic Publishers.